

UC Riverside

UC Riverside Previously Published Works

Title

TensorView for MATLAB: Visualizing tensors with Euler angle decoding.

Permalink

<https://escholarship.org/uc/item/4p4077tg>

Authors

Svenningsson, Leo
Mueller, Leonard

Publication Date

2023-02-01

DOI

10.1016/j.ssnmr.2022.101849

Peer reviewed



Published in final edited form as:

Solid State Nucl Magn Reson. 2023 February ; 123: 101849. doi:10.1016/j.ssnmr.2022.101849.

TensorView for MATLAB: Visualizing tensors with Euler angle decoding

Leo Svenningsson^{a,**}, Leonard J. Mueller^{b,*}

^aDivision of Physical Chemistry, Lund University, Lund, Sweden

^bDepartment of Chemistry, University of California, Riverside, CA, USA

Abstract

TensorView for MATLAB is a GUI-based visualization tool for depicting second-rank Cartesian tensors as surfaces on three-dimensional molecular models. Both ellipsoid and ovaloid tensor display formats are supported, and the software allows for easy conversion of Euler angles from common rotation schemes (active, passive, ZXZ, and ZYZ conventions) with visual feedback. In addition, the software displays all four orientation-equivalent Euler angle solutions for the placement of a single tensor in the molecular frame and can report relative orientations of two tensors with all 16 orientation-equivalent Euler angle sets that relate them. The salient relations are derived and illustrated through several examples. TensorView for MATLAB expands and complements the earlier implementation of TensorView within the Mathematica programming environment and can be run without a MATLAB license. TensorView for MATLAB is available through github at <https://github.com/LeoSvenningsson/TensorViewforMatlab>, and can also be accessed directly via the NMRbox resource.

Keywords

tensor; Molecular visualization; Rotation; Relative orientation; Euler angle conversions

1. Introduction

The visualization of tensor properties as surfaces on three-dimensional models highlights the geometric relationship between the tensor components and essential aspects of the underlying molecular and electronic structure [1–7]. In magnetic resonance, the depiction of tensors – such as the chemical shielding/shift, dipolar, quadrupolar, electron g, hyperfine, diffusion, and anisotropic atomic displacement parameters [8–21] – underscores this connection. Such visual representations can be a significant aid in conveying these geometric relationships in scientific communication that is relevant for magnetic resonance as well as other fields, as tensors are ubiquitous across the sciences.

*Corresponding author. leonard.mueller@ucr.edu (L.J. Mueller). **Corresponding author. leo.svenningsson@fkem1.lu.se (L. Svenningsson).

Declaration of competing interest

The authors declare that they have no known competing financial interests or personal relationships that could have appeared to influence the work reported in this paper

Previously, one of us (LJM) published a Mathematica based software tool called TensorView to display second-rank Cartesian tensors directly upon the molecular framework, taking as input the molecular coordinates and tensor elements [5]. Multiple examples were demonstrated, and applications from other labs have shown even more, including ^{11}B , ^{13}C , ^{17}O , ^{19}F , and ^{29}Si chemical shielding/shift tensors [22,23,23–26], ^{17}O and ^{45}Sc quadrupolar coupling tensors [26,27], electron g and hyperfine coupling tensors [17], and atomic root-mean-square displacement tensors (anisotropic displacement parameters) [21]. To enable a still greater number of applications, we have ported the principles of TensorView to MATLAB and constructed a GUI that runs with the free MATLAB compiler on Windows and Mac. The two implementations of TensorView will be distinguished below as TensorView.nb (Mathematica) and Tensorview.mlapp (MATLAB). Tensorview.mlapp reads atom coordinate files in either protein data bank (.pdb) or molecular coordinate (.xyz) format and produces a 3D model of the molecule and a user supplied tensor, which may have been determined experimentally or computationally [28,29]. The 3D model can be exported in .glb and .wrl format for use with dedicated 3D visualization software, such as the free Blender software [30]. The Github repository contains all of the source files and a script version that can be directly built into other MATLAB pipelines. TensorView for MATLAB is also available for ready access through the NMRbox resource [31].

Several issues important to the description and depiction of second-rank Cartesian tensors are first considered below in the context of the Tensorview.mlapp interface, including tensor symmetry, principal axis system, tensor shape, and Euler angle conventions. A more comprehensive discussion of these topics is given in the original TensorView paper [5]. Unique to Tensorview.mlapp is a module that can switch between the common rotation systems: active ZXZ, passive ZXZ, active ZYZ, and passive ZYZ. Active and passive denote if the rotation is applied to the object or the reference frame, respectively, and have been discussed and reviewed extensively [32,33]. Tensorview.mlapp also provides the option to simultaneously display multiple tensors, along with a list of the Euler angles that relate their relative orientation. There are 16 sets of orientation-equivalent Euler angles that describe the same relative orientation of 2 second-rank Cartesian tensors; as an aid to bridge Euler angle information from external sources, Tensorview.mlapp lists them all. These are derived along with several other useful relationships between Euler angles and conventions in Section 5. Finally, in Section 6 we describe in some detail the numerical methods employed in Tensorview.mlapp for the determination of the Euler angles, paying particular attention to the complications that arise for degenerate principal axis components under the various conventions.

2. The MATLAB graphical user interface

The MATLAB based GUI interface of version 1.15 of Tensorview.mlapp is shown in Fig.1 The tensor field uses \mathbf{A} to signify a general 3×3 Cartesian tensor, written in the molecular coordinate frame (\mathbf{A}^{MF}),

$$\text{general form: } \mathbf{A}^{\text{MF}} = \begin{pmatrix} A_{11}^{\text{MF}} & A_{12}^{\text{MF}} & A_{13}^{\text{MF}} \\ A_{21}^{\text{MF}} & A_{22}^{\text{MF}} & A_{23}^{\text{MF}} \\ A_{31}^{\text{MF}} & A_{32}^{\text{MF}} & A_{33}^{\text{MF}} \end{pmatrix} \quad (1)$$

$$\text{symmetric form: } \mathbf{A}^{\text{MF}} = \frac{\mathbf{A} + (\mathbf{A})^{\text{T}}}{2}. \quad (2)$$

Tensors can be entered in either symmetric or general forms, although any operation within the GUI will return the symmetric form with: $A_{12} = A_{21}$, $A_{13} = A_{31}$ and $A_{23} = A_{32}$. Clicking on the “Molecular Frame \rightarrow Euler” button under the central Euler angle tab generates a list of the principal axis system (PAS) components - the eigenvalues of the symmetric component of the tensor. These can be ordered in an ascending or descending form to correspond to the Haeberlen, Mehring, or IUPAC conventions [9,10,34]. The corresponding Euler angles that relate the PAS and molecular frames are given in the chosen rotation convention. In all cases,

$$\mathbf{A}^{\text{MF}} = \mathbf{R}(\alpha, \beta, \gamma) \mathbf{A}^{\text{PAS}} \mathbf{R}^{-1}(\alpha, \beta, \gamma) \quad (3)$$

where

$$\mathbf{A}^{\text{PAS}} = \begin{pmatrix} A_{11}^{\text{PAS}} & 0 & 0 \\ 0 & A_{22}^{\text{PAS}} & 0 \\ 0 & 0 & A_{33}^{\text{PAS}} \end{pmatrix} \quad (4)$$

and R is the rotation matrix. While the definition (and numerical values) of the Euler angles changes within the various rotational conventions, the actual rotation matrix elements themselves will have the same numerical values regardless of the convention chosen [33].

There are several additional options at this point. Clicking on “Molecular Frame \leftarrow Euler” regenerates the molecular frame tensor from the PAS components and Euler angles. Note, however, that this gives only the symmetric tensor components (the anti-symmetric components are not part of the PAS). This operation also provides an alternate manner for entering a tensor using the PAS components and Euler angles. Second, selecting the “Shielding \leftrightarrow Shift” button replaces the PAS components with their negative values plus the chemical shift reference, which is entered in the corresponding box. This can be used to subsequently generate the chemical shift tensor, δ , in the molecular frame from an initial chemical shielding tensor, σ , or *vice versa*. The central “Dipolar tensor” tab can also be used to generate a dipolar tensor in the molecular frame directly from the coordinates of two atoms. Note that this tensor is normalized with PAS components of -1 , -1 , and 2 .

TensorView supports two conventions for the display of tensor surfaces: the historic ellipsoidal representation [10], and the more technically correct ovaloid form [5,35,36]. An example of the two display formats is shown in Fig. 2, where the differences between the ovaloid and ellipsoidal surfaces are apparent. The ovaloid form is the actual shape of a

symmetric second-rank Cartesian tensor, meaning that the distance from the tensor center to any point on the surface is proportional to the strength of the interaction (shielding here) when the magnetic field is applied along that direction in space. This shape was originally noted by Hansen and Bouman [35] as well as Radaglia [36] and Aschbach [37], and the equation for this surface has been written down explicitly by Young et al. [5]. The ellipsoidal representation is ubiquitous in the NMR literature, but can be misleading since the model does not appropriately accommodate the combination of positive and negative tensor values. Still, its prevalence argues for inclusion as a display option, and it may be preferred for aesthetic reasons in certain cases.

Fig. 2 also highlights that the tensors themselves are symmetric with respect to 180° rotations about the PAS X, Y, or Z axes. Thus, the Euler angles for positioning the tensor in the molecular frame are not unique [5], and Tensorview.mlapp list all 4 orientation-equivalent Euler angle solutions under “Equivalent Angles.” Here equivalent does not mean that the rotation matrices are the same, but rather that they all produce the equivalent molecular frame tensors from the PAS components and the given Euler angles according to Eq. (3). This point is discussed in more detail in Section 4.

To display the tensor on the molecular model, one first imports a coordinate file using the top left “Load” button and enters the molecular coordinates for centering the tensor under “Tensor coordinates.” The tensor size relative to the molecule is set through the “Tensor scaling,” which is the scaled length of the largest principal axis component in units of Angstroms. “Get 3D model” opens the MATLAB 3D display window with the chosen elements rendered (molecule and/or tensor).

Tensorview.mlapp has the ability to display multiple tensors simultaneously. Additional tensors can be added to the 3D object by selecting the “Additional tensors” check box, adding the tensor details, and executing “Get 3D model.” A relative scaling can be applied when displaying multiple tensors by adjusting the “Tensor scaling” value. As new tensors are generated they can be added to the tensor list pane on the right for easy recall using “Tensor \rightarrow List” and “Tensor \leftarrow List,” respectively. The tensor lists can be saved from the pane as well. Users are encouraged to open the simple text files and may find them a convenient route for bringing in multiple tensors for display, along with their placement, scaling, and color. Although at this point TensorView.mlapp does not support direct import from the various computational program output files, the simple nature of the data file allows for facile creation either by hand or with custom scripts that can be tailored to the end users’ specific interest.

3. Examples of tensors from theory and experiment

As a first example, Fig. 3 depicts the chemical shielding tensor for the side branching carbon on the thiophene ring in the electrically conductive polymer poly(3-hexylthiophene) (P3HT). This tensor and its orientation were derived experimentally [38]. For electrically conductive macromolecules such as this [39,40], electron mobility is partially correlated with the residual dipolar coupling tensor [41]. At the same time, anisotropic conductivity is correlated to the molecular orientation distribution [42], which can be inferred from the

chemical shift anisotropy [14,15]. Both the chemical shift principal axis components and the tensor orientation (Euler angles) relative to the molecular frame are crucial in the study of macromolecular anisotropy of films and fibers using NMR.

As a second example, Fig. 4 shows one the backbone amide chemical shielding tensors in the tripeptide Ala-Ala-Ala, calculated by Young et al. [5]. The least shielded component, σ_{11} , lies in the amide plane and is tilted by 18° from the N–H bond vector. The most shielded component, σ_{33} , is found to be nearly perpendicular to the peptide plane, while σ_{22} lies close to the plane. This contrasts with Gly-Gly, where the σ_{33} and σ_{22} components are rotated by ca. 90° about the axis of σ_{11} [43]. For peptides, σ_{11} is found in general to remain within a few degrees of this orientation, while σ_{22} and σ_{33} vary as the secondary structure and amino acid composition change [43].

4. Multiple tensors and relative orientations

The multiple-tensor display feature highlights the relative orientations of tensors to the molecular frame as well as to each other. The relative orientation of tensors plays critical roles in describing tensor correlation experiments in solid state NMR [44–46] and in the analysis of cross-correlated relaxation effects in TROSY and quadrupolar central transition (QCT) NMR in solution [47,48]. For example, Fig. 5(a) shows the relative orientation of the ^{17}O quadrupolar and chemical shielding tensors for the carboxylate group of the bound α -aminoacrylate intermediate in the active site of the enzyme tryptophan synthase [49]. Here, both the magnitudes and the orientations of the tensors come into play in analyzing the ^{17}O QCT NMR data [48]. Multiple programs, including TensorView.nb [5] and EFGShield [2], can report the relative orientation of two tensors. In this case, TensorView.nb reports the relative orientation of the shielding tensor in the PAS of the EFG tensor as $\mathbf{\Omega}_{\text{CS}}^{\text{EFG}} = [\alpha = 4.1^\circ, \beta = 89.7^\circ, \gamma = 154.7^\circ]$. EFGShield reports the same relative orientation as $\mathbf{\Omega}_{\text{CS}}^{\text{EFG}} = [\alpha = 175.9^\circ, \beta = 89.7^\circ, \gamma = 205.1^\circ]$. Both programs state that they are using the same active ZYZ rotational convention with shielding eigenvalues sorted according to $\sigma_{33} > \sigma_{22} > \sigma_{11}$ and the EFG sorted as $|V_{33}| > |V_{22}| > |V_{11}|$. At first these seem inconsistent, but by using Tensorview.mlapp to display the EFG and shielding tensors in the PAS of the EFG tensor (in which case $\mathbf{\Omega}_{\text{EFG}}^{\text{EFG}} = [\alpha = 0^\circ, \beta = 0^\circ, \gamma = 0^\circ]$ and $\mathbf{\Omega}_{\text{CS}}^{\text{EFG}}$ are given above), it can be readily verified that the relative orientations are indeed the same, although the absolute orientations of the PAS are rotated (Fig. 5(b)). There are in fact 16 orientation-equivalent Euler angle sets that describe the relative orientation of two symmetric second-rank tensors. These correspond to the four possible ways of placing the PAS axes on each tensor [5]. As reconciling the various reported Euler angles for a single tensor in the molecular frame or the relative orientation of two tensors can be a challenge, we detail the general relationships for equivalent Euler angle sets in the following section.

5. Orientation-equivalent Euler angle sets

5.1. A few conventions and important relations

By convention Euler angles are chosen such that

$$0 \leq \alpha \leq 2\pi \quad (5)$$

$$0 \leq \beta \leq \pi \quad (6)$$

$$0 \leq \gamma \leq 2\pi \quad (7)$$

Should either α or γ fall outside that range they can be adjusted by adding multiples of 2π . Negative values of β may similarly be adjusted, while $\pi \leq \beta \leq 2\pi$ can be converted by noting that in both the active and passive ZYZ and ZXZ rotation conventions

$$\mathbf{R}(\alpha, \beta, \gamma) = \mathbf{R}(\alpha + \pi, 2\pi - \beta, \gamma + \pi) \quad (8)$$

It is also handy to note the following relationships between active and passive rotations:

$$\mathbf{R}_{\text{active}}(\alpha, \beta, \gamma) = \mathbf{R}_{\text{passive}}(-\gamma, -\beta, -\alpha) = \mathbf{R}_{\text{passive}}(\pi - \gamma, \beta, \pi - \alpha) \quad (9)$$

And the simple relationship between the ZYZ and ZXZ conventions (both active and passive) [50]:

$$\mathbf{R}_{\text{ZYZ}}(\alpha, \beta, \gamma) = \mathbf{R}_{\text{ZXZ}}(\alpha + \pi/2, \beta, \gamma - \pi/2) \quad (10)$$

$$\mathbf{R}_{\text{ZXZ}}(\alpha, \beta, \gamma) = \mathbf{R}_{\text{ZYZ}}(\alpha - \pi/2, \beta, \gamma + \pi/2) \quad (11)$$

All of the above can be verified by direct substitution into the corresponding rotation matrices, which are explicitly written out in their active forms in Section 6. Other conventions for describing orientations and rotations, such as the direction cosine matrix [50] and Cayley-Klein parameters/quaternions [50,51], are potential features for future versions of TensorView.mlapp.

5.2. The rotation of a single 2nd rank tensor

As described in the original TensorView paper, the symmetry of a second-rank Cartesian tensor to 180° rotations about each of the PAS axes leads to a set of 4 orientation-equivalent Euler angles solutions relating the lab and PAS frames [5]. By this, we mean that any choice of Euler angles from this set leads to an equivalent physical orientation of the tensor in the lab frame (although the PAS axes may point in different directions); or, said another way, that the application of the corresponding rotation matrices results in the same lab frame tensor as given in Eq. (3). This set of angles can be solved for by finding the angles that satisfy the following equations in which an initial 180° rotation is given about an axis aligned along the PAS X, Y, and Z axes prior to the general rotation $\Omega = [\alpha, \beta_1, \gamma_1]$.

$$\mathbf{R}(\alpha_1, \beta_1, \gamma_1) \quad (12)$$

$$\mathbf{R}(\alpha_2, \beta_2, \gamma_2) = \mathbf{R}(\alpha_1, \beta_1, \gamma_1)\mathbf{R}_x(\pi) \quad (13)$$

$$\mathbf{R}(\alpha_3, \beta_3, \gamma_3) = \mathbf{R}(\alpha_1, \beta_1, \gamma_1)\mathbf{R}_y(\pi) \quad (14)$$

$$\mathbf{R}(\alpha_4, \beta_4, \gamma_4) = \mathbf{R}(\alpha_1, \beta_1, \gamma_1)\mathbf{R}_z(\pi) \quad (15)$$

Because of the order in which the rotations are given, the initial π rotation can be written in either the lab (xyz) or PAS (XYZ) frames - they are equivalent at this point.

For the active ZYZ rotation convention, the orientation-equivalent rotations correspond to

$$\mathbf{\Omega}_1 = [\alpha_1, \beta_1, \gamma_1] \quad (16)$$

$$\mathbf{\Omega}_2 = [\alpha_2, \beta_2, \gamma_2] = [\alpha_1 + \pi, \pi - \beta_1, 2\pi - \gamma_1] \quad (17)$$

$$\mathbf{\Omega}_3 = [\alpha_3, \beta_3, \gamma_3] = [\alpha_1 + \pi, \pi - \beta_1, \pi - \gamma_1] \quad (18)$$

$$\mathbf{\Omega}_4 = [\alpha_4, \beta_4, \gamma_4] = [\alpha_1, \beta_1, \gamma_1 + \pi], \quad (19)$$

while for the passive ZYZ convention, they are

$$\mathbf{\Omega}_1 = [\alpha_1, \beta_1, \gamma_1] \quad (20)$$

$$\mathbf{\Omega}_2 = [\alpha_2, \beta_2, \gamma_2] = [2\pi - \alpha_1, \pi - \beta_1, \gamma_1 + \pi] \quad (21)$$

$$\mathbf{\Omega}_3 = [\alpha_3, \beta_3, \gamma_3] = [\pi - \alpha_1, \pi - \beta_1, \gamma_1 + \pi] \quad (22)$$

$$\mathbf{\Omega}_4 = [\alpha_4, \beta_4, \gamma_4] = [\alpha_1 + \pi, \beta_1, \gamma_1]. \quad (23)$$

The same solutions hold for the active and passive ZXZ conventions, respectively, although the association with the rotations is switched for $\mathbf{\Omega}_2$ and $\mathbf{\Omega}_3$. Note that if the initial set of Euler angle $\mathbf{\Omega}_1 = [\alpha_1, \beta_1, \gamma_1]$ satisfies

$$0 \leq \alpha_1 \leq \pi \quad (24)$$

$$0 \leq \beta_1 \leq \pi \quad (25)$$

$$0 \leq \gamma_1 \leq \pi \quad (26)$$

(which is always one of the solutions) then the orientation-equivalent Euler angles will fall within the canonical ranges.

It is important to note that there will be additional orientation-equivalent Euler angle sets when the tensor itself is axially symmetric, with any two of the tensor principal components equal. This degeneracy leads to an unconstrained degree of freedom in specifying the orientation. For example, when the unique principal component is along the Z-axis, the γ Euler angle is unconstrained and can be chosen arbitrarily in the active ZYZ and ZXZ conventions; similarly for the α angle in the passive conventions. This means that any choice of those angles will result in the same orientation for the tensor in the molecular frame, or the same lab frame tensor according to Eq. (3). When the unique component is chosen to define the PAS X axis, there is no simple mapping of the degree of freedom to a single Euler angle. This will be discussed in more detail in Section 6.

5.3. The relative orientation of two 2nd rank tensors

To describe the orientation of tensor \mathbf{B} in the PAS of tensor \mathbf{A} , denoted $\mathbf{B}^{\mathbf{A}}$, we begin by aligning the system such that the PAS of tensor \mathbf{A} corresponds to the laboratory frame and describe the orientation of tensor \mathbf{B} within that frame using the Euler angles in the usual way. In this case

$$\mathbf{A}^{\text{lab}} = \mathbf{A}^{\text{PAS}} = \mathbf{A}^{\mathbf{A}} = \mathbf{R}_{\mathbf{A}}^{-1} \mathbf{A}^{\text{MF}} \mathbf{R}_{\mathbf{A}} \quad (27)$$

and

$$\mathbf{B}^{\mathbf{A}} = \mathbf{R}_{\mathbf{A}}^{-1} \mathbf{B}^{\text{MF}} \mathbf{R}_{\mathbf{A}} \quad (28)$$

The relative orientation of \mathbf{B} to \mathbf{A} is defined by the rotation of tensor \mathbf{B} such that

$$\mathbf{B}^{\mathbf{A}} = \mathbf{R}_{\text{rel}} \mathbf{B}^{\mathbf{B}} \mathbf{R}_{\text{rel}}^{-1} \quad (29)$$

Considering that

$$\mathbf{B}^{\text{MF}} = \mathbf{R}_{\mathbf{B}} \mathbf{B}^{\mathbf{B}} \mathbf{R}_{\mathbf{B}}^{-1} \quad (30)$$

and inserting equations (29) and (30) into (28) we obtain the relative rotation matrix

$$\mathbf{R}_{\text{rel}} = \mathbf{R}_{\mathbf{A}}^{-1} \mathbf{R}_{\mathbf{B}} \quad (31)$$

There are 4 orientation-equivalent Euler angle sets for both $\mathbf{R}_{\mathbf{A}}$ and $\mathbf{R}_{\mathbf{B}}$. As described above, these correspond to an initial π rotation of the system about an axis aligned along the tensor PAS X, Y, or Z axis. The full set of relative orientation-equivalent Euler angles relating the orientation of tensor \mathbf{B} in the PAS of tensor \mathbf{A} can therefore be determined by finding the angles that satisfy the following equations:

$$\mathbf{R}(\alpha_1, \beta_1, \gamma_1) = \mathbf{R}_{\text{rel}} = \mathbf{R}_{\mathbf{A}}^{-1} \mathbf{R}_{\mathbf{B}} \quad (32)$$

$$\mathbf{R}(\alpha_2, \beta_2, \gamma_2) = \mathbf{R}(\alpha_1, \beta_1, \gamma_1) \mathbf{R}_{\mathbf{A}}(\pi) \quad (33)$$

$$\mathbf{R}(\alpha_3, \beta_3, \gamma_3) = \mathbf{R}(\alpha_1, \beta_1, \gamma_1)\mathbf{R}_y(\pi) \quad (34)$$

$$\mathbf{R}(\alpha_4, \beta_4, \gamma_4) = \mathbf{R}(\alpha_1, \beta_1, \gamma_1)\mathbf{R}_z(\pi) \quad (35)$$

$$\mathbf{R}(\alpha_5, \beta_5, \gamma_5) = \mathbf{R}_x(\pi)\mathbf{R}(\alpha_1, \beta_1, \gamma_1) \quad (36)$$

$$\mathbf{R}(\alpha_6, \beta_6, \gamma_6) = \mathbf{R}_x(\pi)\mathbf{R}(\alpha_1, \beta_1, \gamma_1)\mathbf{R}_x(\pi) \quad (37)$$

$$\mathbf{R}(\alpha_7, \beta_7, \gamma_7) = \mathbf{R}_x(\pi)\mathbf{R}(\alpha_1, \beta_1, \gamma_1)\mathbf{R}_y(\pi) \quad (38)$$

$$\mathbf{R}(\alpha_8, \beta_8, \gamma_8) = \mathbf{R}_x(\pi)\mathbf{R}(\alpha_1, \beta_1, \gamma_1)\mathbf{R}_z(\pi) \quad (39)$$

$$\mathbf{R}(\alpha_9, \beta_9, \gamma_9) = \mathbf{R}_y(\pi)\mathbf{R}(\alpha_1, \beta_1, \gamma_1) \quad (40)$$

$$\mathbf{R}(\alpha_{10}, \beta_{10}, \gamma_{10}) = \mathbf{R}_y(\pi)\mathbf{R}(\alpha_1, \beta_1, \gamma_1)\mathbf{R}_x(\pi) \quad (41)$$

$$\mathbf{R}(\alpha_{11}, \beta_{11}, \gamma_{11}) = \mathbf{R}_y(\pi)\mathbf{R}(\alpha_1, \beta_1, \gamma_1)\mathbf{R}_y(\pi) \quad (42)$$

$$\mathbf{R}(\alpha_{12}, \beta_{12}, \gamma_{12}) = \mathbf{R}_y(\pi)\mathbf{R}(\alpha_1, \beta_1, \gamma_1)\mathbf{R}_z(\pi) \quad (43)$$

$$\mathbf{R}(\alpha_{13}, \beta_{13}, \gamma_{13}) = \mathbf{R}_z(\pi)\mathbf{R}(\alpha_1, \beta_1, \gamma_1) \quad (44)$$

$$\mathbf{R}(\alpha_{14}, \beta_{14}, \gamma_{14}) = \mathbf{R}_z(\pi)\mathbf{R}(\alpha_1, \beta_1, \gamma_1)\mathbf{R}_x(\pi) \quad (45)$$

$$\mathbf{R}(\alpha_{15}, \beta_{15}, \gamma_{15}) = \mathbf{R}_z(\pi)\mathbf{R}(\alpha_1, \beta_1, \gamma_1)\mathbf{R}_y(\pi) \quad (46)$$

$$\mathbf{R}(\alpha_{16}, \beta_{16}, \gamma_{16}) = \mathbf{R}_z(\pi)\mathbf{R}(\alpha_1, \beta_1, \gamma_1)\mathbf{R}_z(\pi) \quad (47)$$

Again because of the order in which the rotations are given, the first π rotation can be written in either the coordinate frame of the lab (xyz) or the PAS of tensor B (XYZ). The final rotation, however, must be written in the lab frame, which corresponds to the PAS of tensor A. For the active ZYZ convention, the relative-orientation equivalent Euler angle set corresponds to:

$$\mathbf{\Omega}_1 = [\alpha_1, \beta_1, \gamma_1] \quad (48)$$

$$\mathbf{\Omega}_2 = [\alpha_2, \beta_2, \gamma_2] = [\alpha_1 + \pi, \pi - \beta_1, 2\pi - \gamma_1] \quad (49)$$

$$\mathbf{\Omega}_3 = [\alpha_3, \beta_3, \gamma_3] = [\alpha_1 + \pi, \pi - \beta_1, \pi - \gamma_1] \quad (50)$$

$$\mathbf{\Omega}_4 = [\alpha_4, \beta_4, \gamma_4] = [\alpha_1, \beta_1, \gamma_1 + \pi] \quad (51)$$

$$\mathbf{\Omega}_5 = [\alpha_5, \beta_5, \gamma_5] = [2\pi - \alpha_1, \pi - \beta_1, \gamma_1 + \pi] \quad (52)$$

$$\mathbf{\Omega}_6 = [\alpha_6, \beta_6, \gamma_6] = [\pi - \alpha_1, \beta_1, \pi - \gamma_1] \quad (53)$$

$$\mathbf{\Omega}_7 = [\alpha_7, \beta_7, \gamma_7] = [\pi - \alpha_1, \beta_1, 2\pi - \gamma_1] \quad (54)$$

$$\mathbf{\Omega}_8 = [\alpha_8, \beta_8, \gamma_8] = [2\pi - \alpha_1, \pi - \beta_1, \gamma_1] \quad (55)$$

$$\mathbf{\Omega}_9 = [\alpha_9, \beta_9, \gamma_9] = [\pi - \alpha_1, \pi - \beta_1, \gamma_1 + \pi] \quad (56)$$

$$\mathbf{\Omega}_{10} = [\alpha_{10}, \beta_{10}, \gamma_{10}] = [2\pi - \alpha_1, \beta_1, \pi - \gamma_1] \quad (57)$$

$$\mathbf{\Omega}_{11} = [\alpha_{11}, \beta_{11}, \gamma_{11}] = [2\pi - \alpha_1, \beta_1, 2\pi - \gamma_1] \quad (58)$$

$$\mathbf{\Omega}_{12} = [\alpha_{12}, \beta_{12}, \gamma_{12}] = [\pi - \alpha_1, \pi - \beta_1, \gamma_1] \quad (59)$$

$$\mathbf{\Omega}_{13} = [\alpha_{13}, \beta_{13}, \gamma_{13}] = [\alpha_1 + \pi, \beta_1, \gamma_1] \quad (60)$$

$$\mathbf{\Omega}_{14} = [\alpha_{14}, \beta_{14}, \gamma_{14}] = [\alpha_1, \pi - \beta_1, 2\pi - \gamma_1] \quad (61)$$

$$\mathbf{\Omega}_{15} = [\alpha_{15}, \beta_{15}, \gamma_{15}] = [\alpha_1, \pi - \beta_1, \pi - \gamma_1] \quad (62)$$

$$\mathbf{\Omega}_{16} = [\alpha_{16}, \beta_{16}, \gamma_{16}] = [\alpha_1 + \pi, \beta_1, \gamma_1 + \pi] \quad (63)$$

This set of relative-orientation equivalent Euler angles also applies to the passive ZYZ convention and both the active and passive ZXZ conventions (although the numerical values of the angles change with the various conventions). These are all of the possible solutions when each of the tensors has no degenerate principal components. When degenerate components are present, there will be additional relative-orientation equivalent solutions that reflect the degrees of freedom in the choice of the Euler angles as discussed in the following

section. Tensorview.mlapp lists all 16 orientation-equivalent Euler angle sets for the relative orientation of two tensors under the “Relative tensors” tab. This data can be exported using the “Save Relative Angles” button.

Returning to the example above for the aminoacrylate intermediate in tryptophan synthase, TensorView.nb reports a relative orientation of $\mathbf{\Omega}_{CS}^{EFG} = [\alpha_1 = 4.1^\circ, \beta_1 = 89.7^\circ, \gamma_1 = 154.7^\circ]$ in the PAS of the EFG tensor. EFGShield reports the same relative orientation as $\mathbf{\Omega}_{CS}^{EFG} = [\alpha_2 = 175.9^\circ, \beta_2 = 89.7^\circ, \gamma_2 = 205.1^\circ]$. Using the equivalence set above, we can now verify that these two sets of Euler angles correspond to the same relative orientation.

6. Tensor symmetries and the numerical calculation of Euler angles

The fundamental design principles and approach of TensorView have already been described by Mueller [5]. Tensorview.mlapp follows many of the same conventions but takes a different approach to the calculation of Euler angles. The numerical methods employed in Tensorview.mlapp are briefly described below, with particular attention paid to the complications that arise for degenerate principal axis components under the various conventions.

The molecular frame tensor can be decomposed into its principal axis components from its eigenvalues, and the rotation matrix is derived from the sorted eigenvectors corresponding to the chosen ascending or descending order of the PAS tensor,

$$\mathbf{A}^{MF} = \mathbf{R}(\alpha, \beta, \gamma) \mathbf{A}^{PAS} \mathbf{R}^{-1}(\alpha, \beta, \gamma) \quad (64)$$

From the rotation matrix, *i.e.*, the eigenvectors, we can find the Euler angles by inference to the matrix elements.

As an example, consider the active ZYZ Euler rotation matrix

$$\begin{aligned} \mathbf{R}_{\text{active}}^{ZY}(\alpha, \beta, \gamma) &= \mathbf{R}_z(\alpha) \mathbf{R}_y(\beta) \mathbf{R}_z(\gamma) \\ &= \begin{pmatrix} \cos \alpha & -\sin \alpha & 0 \\ \sin \alpha & \cos \alpha & 0 \\ 0 & 0 & 1 \end{pmatrix} \begin{pmatrix} \cos \beta & 0 & \sin \beta \\ 0 & 1 & 0 \\ -\sin \beta & 0 & \cos \beta \end{pmatrix} \begin{pmatrix} \cos \gamma & -\sin \gamma & 0 \\ \sin \gamma & \cos \gamma & 0 \\ 0 & 0 & 1 \end{pmatrix} \\ &= \begin{pmatrix} \cos \alpha \cos \beta \cos \gamma - \sin \alpha \sin \gamma & -\sin \alpha \cos \gamma - \cos \alpha \cos \beta \sin \gamma & \cos \alpha \sin \beta \\ \sin \alpha \cos \beta \cos \gamma + \cos \alpha \sin \gamma & \cos \alpha \cos \gamma - \sin \alpha \cos \beta \sin \gamma & \sin \alpha \sin \beta \\ -\sin \beta \cos \gamma & \sin \beta \sin \gamma & \cos \beta \end{pmatrix} \end{aligned} \quad (65)$$

From Equation (65) we can easily calculate β since:

$$\beta = \cos^{-1}(\mathbf{R}_{33}) \quad (66)$$

The variables α and γ are less obvious since we have to sort out the multitude of solutions that go with β [52]. One way to solve all cases when $\cos \beta \neq 0$ is shown in Equations (67) and (68). The MATLAB atan2 function takes into account the individual signs of the usual y/x form of the tangent function. The resulting angle is then determined between $[-\pi, \pi]$.

$$\alpha = \text{atan2}\left(\frac{\mathbf{R}_{22}}{\sin(\beta)}, \frac{\mathbf{R}_{13}}{\sin(\beta)}\right) \quad (67)$$

$$\gamma = \text{atan2}\left(\frac{\mathbf{R}_{32}}{\sin(\beta)}, \frac{-\mathbf{R}_{31}}{\sin(\beta)}\right) \quad (68)$$

If $\beta = 0$, also known as a ‘‘gimbal lock’’ in some fields, the two rotations α and γ revolves around the same axis, so we choose $\gamma = 0$, and α is calculated as

$$\alpha = \cos^{-1}(\mathbf{R}_{11}) \text{ if } \beta = 0. \quad (69)$$

A special case occurs for the symmetrical eigenvalue in the form $A_{11}^{\text{PAS}} = A_{22}^{\text{PAS}}$ or $A_{22}^{\text{PAS}} = A_{33}^{\text{PAS}}$, depending on how they are sorted. In an active rotation with the unique axis in the Z-direction, i.e., $A_{11}^{\text{PAS}} = A_{22}^{\text{PAS}}$, the last rotation around A_{33}^{PAS} by γ is unconstrained and can be set to 0. Conversely, when the eigenvalues are sorted with the unique axis in the X-direction, i.e., $A_{22}^{\text{PAS}} = A_{33}^{\text{PAS}}$, no easy simplification of the solution can be made due to degenerate solutions on a non-intuitive symmetry line. The eigenvalue solver in MATLAB will find one (correct) solution based on floating point jittering, though it is challenging to compare with other software and solutions in such conditions. We therefore do not take this approach. Instead one can find solutions for $\alpha = 0$ in the equality for the active ZYZ rotation:

$$\mathbf{A}^{\text{MF}} = \mathbf{R}_{\text{active}}(0, \beta, \gamma) \mathbf{A}^{\text{PAS}} \mathbf{R}_{\text{active}}^{-1}(0, \beta, \gamma) \quad (70)$$

Where solutions can be found from elements of the tensor valued Equation (70), for example:

$$A_{22}^{\text{MF}} = A_{22}^{\text{PAS}} + A_{11}^{\text{PAS}} \sin^2 \gamma - A_{22}^{\text{PAS}} \sin^2 \gamma \quad (71)$$

Two solution can be found from solving

$$\gamma = \sin^{-1}\left(\pm \sqrt{\frac{A_{22}^{\text{MF}} - A_{22}^{\text{PAS}}}{A_{11}^{\text{PAS}} - A_{22}^{\text{PAS}}}}\right) \quad (72)$$

And then β is calculated from

$$\beta = \text{atan2}\left(\frac{-A_{23}^{\text{MF}}}{\sin(\gamma)\cos(\gamma)(A_{11}^{\text{PAS}} - A_{22}^{\text{PAS}})}, \frac{A_{12}^{\text{MF}}}{\sin(\gamma)\cos(\gamma)(A_{11}^{\text{PAS}} - A_{22}^{\text{PAS}})}\right) \quad (73)$$

Only one solution for β is correct for a chosen γ which we select as the positive solutions for γ . If $A_{23}^{\text{MF}} = A_{12}^{\text{MF}} = 0$ we can solve

$$\beta = \sin^{-1}\left(\pm \sqrt{\frac{A_{33}^{\text{MF}} - A_{33}^{\text{PAS}}}{A_{11}^{\text{PAS}} - A_{33}^{\text{PAS}} + (A_{22}^{\text{PAS}} - A_{11}^{\text{PAS}})\sin^2 \gamma}}\right) \quad (74)$$

with the solutions crosschecked against \mathbf{A}^{MF} . Also observing that degenerate solutions for β exists for $\gamma = \pm \pi/2$, we can choose $\beta = 0$.

For active ZXZ, with

$$\begin{aligned} \mathbf{R}_{\text{active}}^{\text{ZXZ}}(\alpha, \beta, \gamma) &= \mathbf{R}_z(\alpha)\mathbf{R}_x(\beta)\mathbf{R}_z(\gamma) \\ &= \begin{pmatrix} \cos \alpha & -\sin \alpha & 0 \\ \sin \alpha & \cos \alpha & 0 \\ 0 & 0 & 1 \end{pmatrix} \begin{pmatrix} 1 & 0 & 0 \\ 0 & \cos \beta & -\sin \beta \\ 0 & \sin \beta & \cos \beta \end{pmatrix} \begin{pmatrix} \cos \gamma & -\sin \gamma & 0 \\ \sin \gamma & \cos \gamma & 0 \\ 0 & 0 & 1 \end{pmatrix} \\ &= \begin{pmatrix} \cos \alpha \cos \gamma - \sin \alpha \cos \beta \sin \gamma & -\sin \alpha \cos \beta \cos \gamma - \cos \alpha \sin \gamma & \sin \alpha \sin \beta \\ \cos \alpha \cos \beta \sin \gamma + \sin \alpha \cos \gamma & \cos \alpha \cos \beta \cos \gamma - \sin \alpha \sin \gamma & -\cos \alpha \sin \beta \\ \sin \beta \sin \gamma & \sin \beta \cos \gamma & \cos \beta \end{pmatrix}, \end{aligned} \quad (75)$$

we similarly obtain

$$\gamma = \sin^{-1} \left(\pm \sqrt{\frac{A_{11}^{\text{MF}} - A_{11}^{\text{PAS}}}{A_{22}^{\text{PAS}} - A_{11}^{\text{PAS}}}} \right) \quad (76)$$

and

$$\beta = \text{atan2} \left(\frac{A_{31}^{\text{MF}}}{\sin(\gamma) \cos(\gamma) (A_{11}^{\text{PAS}} - A_{22}^{\text{PAS}})}, \frac{A_{21}^{\text{MF}}}{\sin(\gamma) \cos(\gamma) (A_{11}^{\text{PAS}} - A_{22}^{\text{PAS}})} \right) \quad (77)$$

If $A_{31}^{\text{MF}} = A_{21}^{\text{MF}} = 0$ we can solve

$$\beta = \sin^{-1} \left(\pm \sqrt{\frac{A_{22}^{\text{MF}} - A_{22}^{\text{PAS}} + (A_{22}^{\text{PAS}} - A_{11}^{\text{PAS}}) \sin^2 \gamma}{A_{33}^{\text{PAS}} - A_{22}^{\text{PAS}} + (A_{22}^{\text{PAS}} - A_{11}^{\text{PAS}}) \sin^2 \gamma}} \right) \quad (78)$$

again observing that degenerate solutions for β exists for $\gamma = 0$ or $\gamma = \pi$, where we can choose $\beta = 0$.

It is noteworthy that we can also solve active ZYZ equations $A_{22}^{\text{PAS}} = A_{33}^{\text{PAS}}$ by setting $\gamma = 0$ but cannot with an active ZXZ rotation due to the final non-zero rotation (X) being a rotation around the unique axis. The degeneracy of the aforementioned symmetrical tensor problem can introduce confusion when using eigenvalue solvers by finding solutions on a non-intuitive symmetry line. Therefore, readers who seek to solve similar problems on their own should pay particular attention to these cases. Fig. 6 shows an active ZYZ rotation scheme with ascending and descending tensor eigenvalue sorting with the tensors being processed in Blender [30] and the 3D models arranged in PowerPoint.

The procedure to obtain consistent angle solutions must also be considered when calculating relative angles of two tensors. We may have one or two tensors with symmetrical eigenvalues where simplifications from rotational symmetries become somewhat intricate. For axially symmetric relative tensors it is also convenient to find solutions for some angles that can be set to zero. When both tensors are axially symmetric, and a ZYZ rotation is used, we can set $\alpha = 0$ and $\gamma = 0$; the angle β is then

$$\beta = \sin^{-1} \left(\pm \sqrt{\frac{\mathbf{B}_{33}^A - \mathbf{B}_{33}^{\text{PAS}}}{\mathbf{B}_{11}^{\text{PAS}} - \mathbf{B}_{33}^{\text{PAS}}}} \right) \quad (79)$$

which can be derived from Equation (29). For ZXZ rotations we have to resort to a combination of solutions shown in Table 1. The rotations are mainly selected to avoid unnecessary rotations around the symmetrical tensor axis, though we acknowledge that other solutions also exists.

When only one of the two tensors are axially symmetric, we can reuse the “Molecular Frame \rightarrow Euler” pipeline in the following way. If tensor B is axially symmetrical then the relative orientation of tensor B in the PAS of tensor A, \mathbf{B}^A , is used in the pipeline. When tensor A is axially symmetrical we can simply obtain the passive angles for \mathbf{A}^B , *i.e.* the relative orientation of tensor A in the PAS of tensor B, since the reference frame rotation of tensor B is the same as the object rotation of tensor A.

The choices we have made here for how to handle axially symmetric tensors may not correspond to the choices made by other software developers. Ultimately, when checking whether two sets of Euler angles describe equivalent orientations, it may be best to directly compare the results of Eq. (3) or visually inspect the tensor in the molecular frame. When comparing two sets of relative orientations, it may also be most facile to display both sets of tensors and check that one set can be rotated onto the other using visual feedback.

7. Conclusion

TensorView for MATLAB provides a straightforward and intuitive GUI to visualize tensors in a molecular context, while offering tools to explore the intricacies of 3D rotations of second rank tensors using different rotation conventions. The representation of tensor properties directly as 3D surfaces on molecular models highlights the relationship between the physical phenomena and the underlying molecular and electronic structures that can help build molecular level insights and enable effective scientific communication. Several relationships between Euler angles in various conventions have also been derived and written down explicitly to facilitate the comparison of results from various computational and modeling software. TensorView for MATLAB provides a licence-free molecular 3D modelling tool that is universally accessible through Github and within the NMRbox resource.

Acknowledgements

This work was supported in part by grants from the US National Institutes of Health (R01GM137008 and R35GM145369 to LJM).

Data availability

Source and executable files for TensorView for MATLAB are freely available at <https://github.com/LeoSvenningsson/TensorViewforMatlab>. TensorView for MATLAB can also be run via the NMRbox resource by typing “activate_tensorview” within MATLAB.

References

- [1]. Bak M, Schultz R, Vosegaard T, Nielsen NC, Specification and visualization of anisotropic interaction tensors in polypeptides and numerical simulations in biological solid-state NMR, *J. Magn. Reson* 154 (1) (2002) 28–45, 10.1006/jmre.2001.2454. [PubMed: 11820824]
- [2]. Adiga S, Aebi D, Bryce DL, Efgshield — a program for parsing and summarizing the results of electric field gradient and nuclear magnetic shielding tensor calculations, *Can. J. Chem* 85 (7–8) (2007) 496–505, 10.1139/v07-069.
- [3]. Biternas A, Charnock G, Kuprov I, A standard format and a graphical user interface for spin system specification, *J. Magn. Reson* 240 (2014) 124–131, 10.1016/j.jmr.2014.01.004. [PubMed: 24530265]
- [4]. Sturniolo S, Green TF, Hanson RM, Zilka M, Refson K, Hodgkinson P, Brown SP, Yates JR, Visualization and processing of computed solid-state NMR parameters: magresview and magrespython, *Solid State Nucl. Magn. Reson* 78 (2016) 64–70, 10.1016/j.ssnmr.2016.05.004. [PubMed: 27435606]
- [5]. Young RP, Lewis CR, Yang C, Wang L, Harper JK, Mueller LJ, Tensorview: a software tool for displaying NMR tensors, *Magn. Reson. Chem* 57 (5) (2019) 211–223, 10.1002/mrc.4793. [PubMed: 30230009]
- [6]. Rinald A, Wu G, A modified townes-dailey model for interpretation and visualization of nuclear quadrupole coupling tensors in molecules, *J. Phys. Chem.A* 124 (6) (2020) 1176–1186, 10.1021/acs.jpca.0c00439. [PubMed: 31968940]
- [7]. Korenchan DE, Lu J, Levitt MH, Jerschow A, ³¹P nuclear spin singlet lifetimes in a system with switchable magnetic inequivalence: experiment and simulation, *Phys. Chem. Chem. Phys* 23 (2021) 19465–19471, 10.1039/D1CP03085J. [PubMed: 34525141]
- [8]. Abragam A, *The Principles of Nuclear Magnetism*, International Series of Monographs on Physics, Clarendon Press, Oxford, 1961.
- [9]. Haeberlen U, *High Resolution NMR in Solids Selective Averaging*, Academic Press, 1976, 10.1016/B978-0-12-025561-0.50007-1.
- [10]. Mehring M, *Principles of High Resolution NMR in Solids*, Springer-Verla, Berlin; New York, 1983.
- [11]. Mehring M, Weberruss VA, *Object-oriented Magnetic Resonance: Classes and Objects, Calculations and Computations*, Academic Press, 2001.
- [12]. Duer MJ (Ed.), *Introduction to Solid-State NMR Spectroscopy*, first ed., Blackwell Publishing Ltd, Oxford, 2004.
- [13]. Herzfeld J, Berger AE, Sideband intensities in NMR spectra of samples spinning at the magic angle, *J. Chem. Phys* 73 (1980) 6021–6030, 10.1063/1.440136.
- [14]. Harbison GS, Vogt V-D, Spiess HW, Structure and order in partially oriented solids: characterization by 2D-magic-angle-spinning NMR, *J. Chem. Phys* 86 (1986) 1206–1218, 10.1063/1.452265.
- [15]. Chmelka BF, Schmidt-Rohr K, Spiess HW, Molecular orientation distributions in poly(ethylene terephthalate) thin films and fibers from multidimensional DECODER NMR spectroscopy, *Macromolecules* 26 (1993) 2282–2296, 10.1021/ma00061a022.
- [16]. Smith AA, Vogel A, Engberg O, Hildebrand PW, Huster D, A method to construct the dynamic landscape of a bio-membrane with experiment and simulation, *Nat. Commun* 13 (1) (2022) 108, 10.1038/s41467-021-27417-y. [PubMed: 35013165]
- [17]. Saliba EP, Barnes AB, Fast electron paramagnetic resonance magic angle spinning simulations using analytical powder averaging techniques, *J. Chem. Phys* 151 (11) (2019), 114107, 10.1063/1.5113598. [PubMed: 31542017]
- [18]. Topgaard D (Ed.), *Advanced Diffusion Encoding Methods in MRI, New Developments in NMR*, The Royal Society of Chemistry, 2020, 10.1039/9781788019910.
- [19]. Topgaard D, Director orientations in lyotropic liquid crystals: diffusion MRI mapping of the saupe order tensor, *Phys. Chem. Chem. Phys* 18 (2016) 8545–8553, 10.1039/C5CP07251D. [PubMed: 26948308]

- [20]. Hofstetter A, Emsley L, Positional variance in NMR crystallography, *J. Am. Chem. Soc* 139 (7) (2017) 2573–2576, 10.1021/jacs.6b12705. [PubMed: 28146348]
- [21]. Wang L, Uribe-Romo FJ, Mueller LJ, Harper JK, Predicting anisotropic thermal displacements for hydrogens from solid-state NMR: a study on hydrogen bonding in polymorphs of palmitic acid, *Phys. Chem. Chem. Phys* 20 (2018) 8475–8487, 10.1039/C7CP06724K. [PubMed: 29431770]
- [22]. Lu M, Ishima R, Polenova T, Gronenborn AM, ¹⁹F NMR relaxation studies of fluorosubstituted tryptophans, *J. Biomol. NMR* 73 (8) (2019) 401–409, 10.1007/s10858-019-00268-y. [PubMed: 31435857]
- [23]. Huynh W, Taylor JW, Harman WH, Conley MP, Solid-state ¹¹B NMR studies of coinage metal complexes containing a phosphine substituted diboraanthracene ligand, *Dalton Trans.* 50 (2021) 14855–14863, 10.1039/D1DT02981A. [PubMed: 34604875]
- [24]. Sun H, Dwaraknath S, Ling H, Qu X, Huck P, Persson KA, Hayes SE, Enabling materials informatics for ²⁹Si solid-state NMR of crystalline materials, *NPJ Computational Materials* 6 (1) (2020) 53, 10.1038/s41524-0200328-3.
- [25]. Chalek KR, Dong X, Tong F, Kudla RA, Zhu L, Gill AD, Xu W, Yang C, Hartman JD, Magalhães A, Al-Kaysi RO, Hayward RC, Hooley RJ, Beran GJO, Bardeen CJ, Mueller LJ, Bridging photochemistry and photomechanics with NMR crystallography: the molecular basis for the macroscopic expansion of an anthracene ester nanorod, *Chem. Sci* 12 (2021) 453–463, 10.1039/D0SC05118G.
- [26]. Shen J, Tersikh V, Struppe J, Hassan A, Monette M, Hung I, Gan Z, Brinkmann A, Wu G, Solid-state ¹⁷O NMR study of α-d-glucose: exploring new frontiers in isotopic labeling, sensitivity enhancement, and NMR crystallography, *Chem. Sci* 13 (2022) 2591–2603, 10.1039/D1SC06060K. [PubMed: 35340864]
- [27]. Culver DB, Huynh W, Tafazolian H, Conley MP, Solid-state ⁴⁵Sc NMR studies of Cp*₂Sc–OR (R = CMe₂CF₃, CMe(CF₃)₂, C(CF₃)₃, SiPh₃) and relationship to the structure of Cp*₂Sc-sites supported on partially dehydroxylated silica, *Organometallics* 39 (7) (2020) 1112–1122, 10.1021/acs.organomet.9b00840.
- [28]. Svenningsson L, Ludwig A, Mueller LJ, Tensorview for Matlab, 2021 (URL github.com/LeoSvenningsson/TensorViewforMatlab).
- [29]. Ludwig A, Molecule3d, 2021 mathworks.com/matlabcentral/fileexchange/55231-molecoule3d.
- [30]. Community BO, Blender - a 3D Modelling and Rendering Package, Blender Foundation, Stichting Blender Foundation, Amsterdam, 2018. URL, <http://www.blender.org>.
- [31]. Maciejewski MW, Schuyler AD, Gryk MR, Moraru II, Romero PR, Ulrich EL, Eghbalnia HR, Livny M, Delaglio F, Hoch JC, NMRbox: a resource for biomolecular NMR computation, *Biophys. J* 112 (8) (2017) 1529–1534, 10.1016/j.bpj.2017.03.011. [PubMed: 28445744]
- [32]. Bouten M, On the rotation operators in quantum mechanics, *Physica* 42 (4) (1969) 572–580, 10.1016/0031-8914(69)90162-1.
- [33]. Mueller LJ, Tensors and rotations in NMR, concepts in magnetic resonance Part A 38A (5), 2011, pp. 221–235. <https://onlinelibrary.wiley.com/doi/abs/10.1002/cmr.a.20224>.
- [34]. Harris RK, Becker ED, de Menezes SMC, Granger P, Hoffman RE, Zilm KW, Further conventions for NMR shielding and chemical shifts (IUPAC recommendations 2008), *Pure Appl. Chem* 80 (1) (2008) 59–84, 10.1351/pac200880010059.
- [35]. Hansen AE, Bouman TD, Calculation, display, and analysis of the nature of nonsymmetric nuclear magnetic resonance shielding tensors: application to three-membered rings, *J. Chem. Phys* 91 (6) (1989) 3552–3560, 10.1063/1.456887.
- [36]. Radeaglia R, On the pictorial representation of the magnetic screening tensor: ellipsoid or ovaloid? *Solid State Nucl. Magn. Reson* 4 (5) (1995) 317–321, 10.1016/0926-2040(95)00009-F. [PubMed: 7583069]
- [37]. Zurek E, Pickard CJ, Autschbach J, Density functional study of the ¹³C NMR chemical shifts in single-walled carbon nanotubes with stone-wales defects, *J. Phys. Chem. C* 112 (31) (2008) 11744–11750, 10.1021/jp803180v.
- [38]. Svenningsson L, Molecular Orientation in Cellulose Fibers and Composites, PhD. Thesis, Chalmers University of Technology, 2020.

- [39]. Kaloni TP, Giesbrecht PK, Schreckenbach G, Freund MS, Polythiophene: from fundamental perspectives to applications, *Chem. Mater* 29 (24) (2017) 10248–10283, 10.1021/acs.chemmater.7b03035.
- [40]. Seifrid M, Reddy GNM, Chmelka BF, Bazan GC, Insight into the structures and dynamics of organic semiconductors through solid-state NMR spectroscopy, *Nat. Rev. Mater* 5 (2020) 910–930, 10.1038/s41578-020-00232-5.
- [41]. Pascui OF, Lohwasser R, Sommer M, Thelakkat M, Thurn-Albrecht T, Saalwächter K, High crystallinity and nature of crystal-crystal phase transformations in regioregular poly(3-hexylthiophene), *Macromolecules* 43 (22) (2010) 9401–9410, 10.1021/ma102205t.
- [42]. Hynynen J, Järsvall E, Kroon R, Zhang Y, Barlow S, Marder SR, Kemerink M, Lund A, Müller C, Enhanced thermoelectric power factor of tensile drawn poly(3-hexylthiophene), *ACS Macro Lett.* 8 (1) (2019) 70–76, 10.1021/acsmacrolett.8b00820. [PubMed: 30701126]
- [43]. Walling AE, Pargas RE, de Dios AC, Chemical shift tensors in peptides: a quantum mechanical study, *J. Phys. Chem.A* 101 (39) (1997) 7299–7303, 10.1021/jp971783m.
- [44]. Feng X, Lee Y, Sandstrom D, Edén M, Maisel H, Sebald A, Levitt M, Direct determination of a molecular torsional angle by solid-state NMR, *Chem. Phys. Lett* 257 (3) (1996) 314–320, 10.1016/0009-2614(96)00558-1.
- [45]. Hong M, Gross JD, Griffin RG, Site-resolved determination of peptide torsion angle ϕ from the relative orientations of backbone N-H and C-H bonds by solid-state NMR, *J. Phys. Chem. B* 101 (30) (1997) 5869–5874, 10.1021/jp970887u.
- [46]. Perras FA, Widdifield CM, Bryce DL, QUEST—quadrupolar exact software: a fast graphical program for the exact simulation of NMR and NQR spectra for quadrupolar nuclei, *Solid State Nucl. Magn. Reson* 45–46 (2012) 36–44, 10.1016/j.ssnmr.2012.05.002.
- [47]. Pervushin K, Riek R, Wider G, Wüthrich K, Attenuated T_2 relaxation by mutual cancellation of dipole-dipole coupling and chemical shift anisotropy indicates an avenue to NMR structures of very large biological macromolecules in solution, *Proc. Natl. Acad. Sci. USA* 94 (23) (1997) 12366–12371, 10.1073/pnas.94.23.12366. [PubMed: 9356455]
- [48]. Shen J, Tersikh V, Wang X, Hung I, Gan Z, Wu G, A quadrupole-central-transition ^{17}O NMR study of nicotinamide: experimental evidence of cross-correlation between second-order quadrupolar interaction and magnetic shielding anisotropy, *J. Phys. Chem. B* 122 (18) (2018) 4813–4820, 10.1021/acs.jpcc.8b02417. [PubMed: 29683675]
- [49]. Holmes JB, Liu V, Caulkins BG, Hilario E, Ghosh RK, Drago VN, Young RP, Romero JA, Gill AD, Bogie PM, Paulino J, Wang X, Riviere G, Bosken YK, Struppe J, Hassan A, Guidoulianov J, Perrone B, Mentink-Vigier F, Chang C. en A.. Long JR, Hooley RJ, Mueser TC, Dunn MF, Mueller LJ, Imaging active site chemistry and protonation states: NMR crystallography of the tryptophan synthase α -aminoacrylate intermediate, *Proc. Natl. Acad. Sci. USA* 119 (2) (2022) e2109235119, doi: 10.1073/pnas.2109235119. [PubMed: 34996869]
- [50]. Goldstein H (Ed.), *Classical Mechanics*, first ed., Pearson, 1951.
- [51]. Blümich B, Spiess H, Quaternions as a practical tool for the evaluation of composite rotations, *J. Magn. Reson* 61 (2) (1985) 356–362, 10.1016/0022-2364(85)90091-5.
- [52]. Slabaugh G, Computing euler angles from a rotation matrix, URL, http://www.close-range.com/docs/Computing_Euler_angles_from_a_rotation_matrix.pdf, 1999



Fig. 1.
The graphical user interface of TensorView for MATLAB.

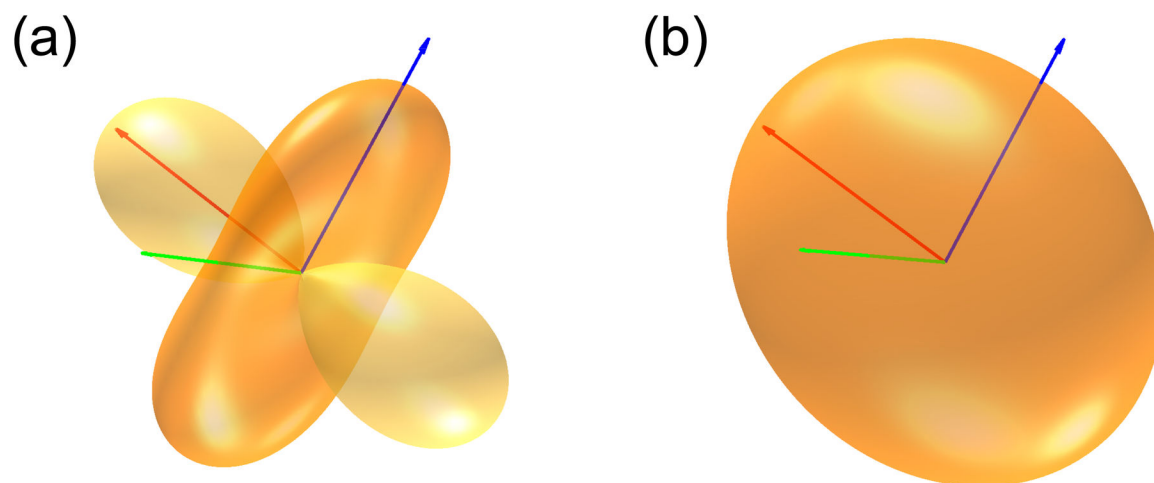


Fig. 2. (a) Ovaloid and (b) ellipsoid representations of a chemical shielding tensor from Ref. [5] in which $\sigma_{11} = -83.2$ ppm, $\sigma_{22} = 43.7$ ppm, and $\sigma_{33} = 66.8$ ppm. The corresponding principal axes are shown in red, green, and blue, respectively. While the use of ellipsoids is ubiquitous in the NMR literature, the true form of a symmetric second-rank Cartesian tensor is an ovaloid.

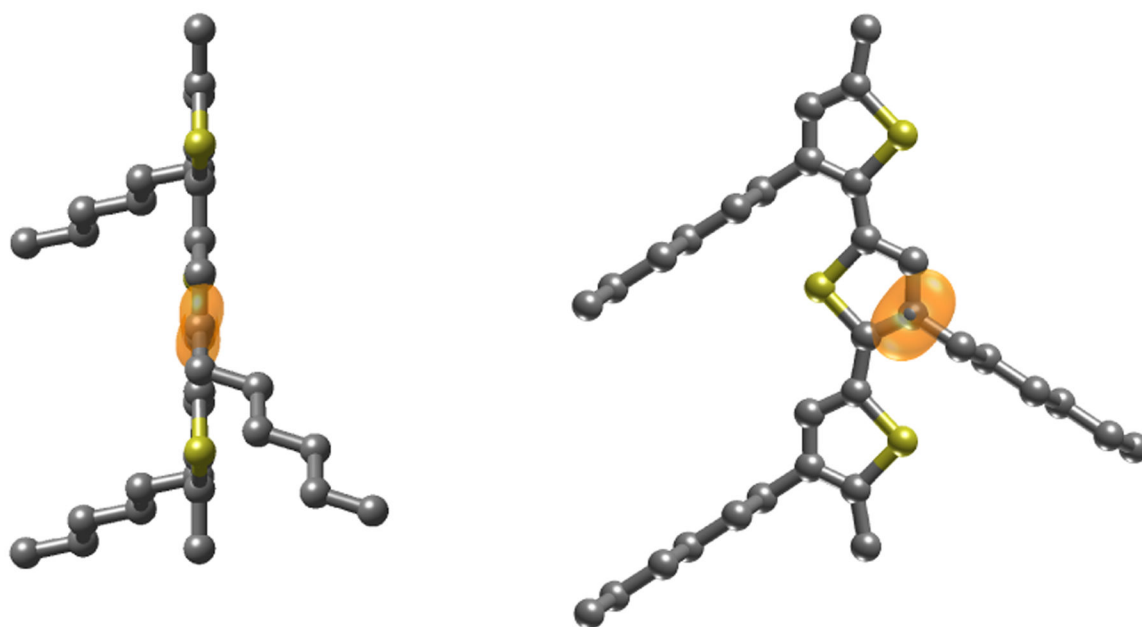


Fig. 3. A polythiophene (P3HT) chain with the chemical shift anisotropy tensor for the side chain branching carbon shown in orange. $\delta_{11} = 215$ ppm, $\delta_{22} = 151$ ppm, and $\delta_{33} = 42$ ppm. The tensor is oriented relative to the molecular frame by passive ZYZ Euler angles $\alpha = 38^\circ$, $\beta = 84^\circ$, and $\gamma = 180^\circ$. Here, the z-axis of the molecular frame defines the polymer backbone.

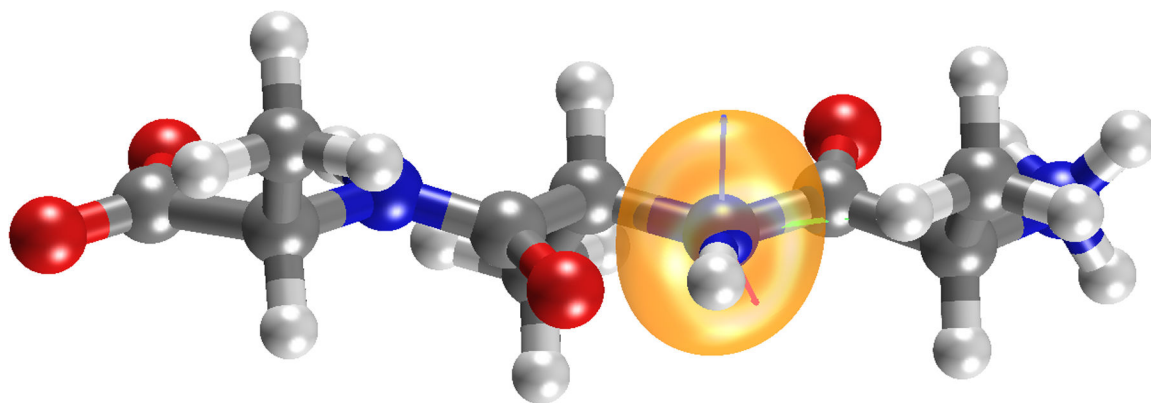


Fig. 4. The tripeptide Ala-Ala-Ala in the extended conformation with backbone torsion angles $\varphi = \psi = 180^\circ$. The backbone amide shielding tensor is shown along with its PAS. The least shielded component lies in the amide plane and is tilted by 18° from the N-H bond vector.

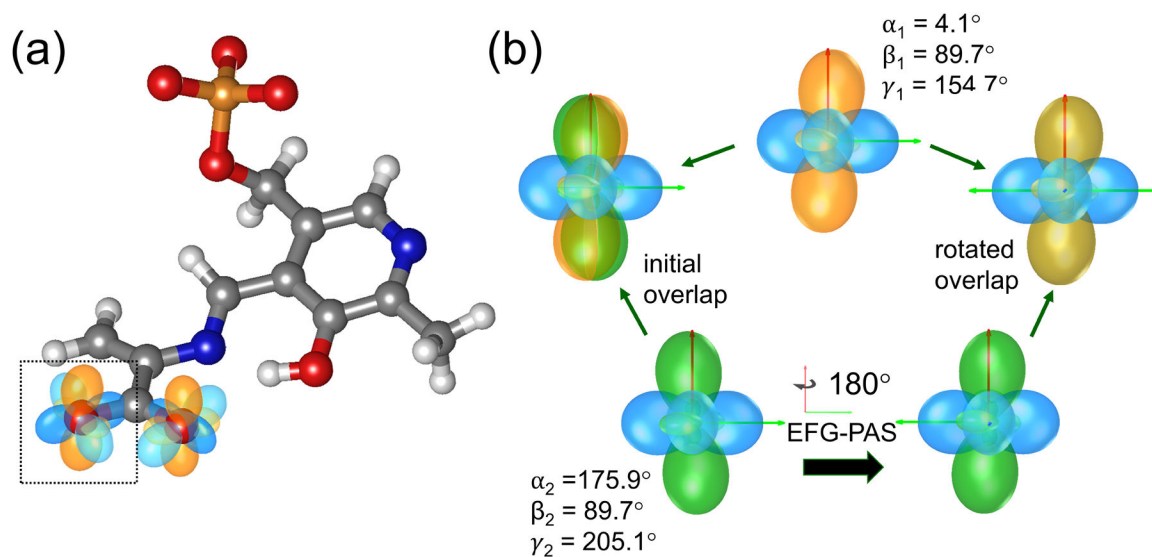


Fig. 5. (a) The ^{17}O quadrupolar (blue) and chemical shielding (orange) tensors for the carboxylate group of the bound α -aminoacrylate intermediate in the active site of the enzyme tryptophan synthase. Concentrating on the distal oxygen, Tensorview.nb reports an orientation of $\mathbf{\Omega}_{\text{CS}}^{\text{EFG}} = [\alpha_1 = 4.1^\circ, \beta_1 = 89.7^\circ, \gamma_1 = 154.7^\circ]$ for the chemical shielding tensor relative to the EFG tensor, while EFGShield reports the relative orientation as $\mathbf{\Omega}_{\text{CS}}^{\text{EFG}} = [\alpha_2 = 175.9^\circ, \beta_2 = 89.7^\circ, \gamma_2 = 205.1^\circ]$ using the same stated conventions. (b) The two relative orientations can be shown to be equivalent by noting that the second system (both EFG and CS) can be superimposed on the first after a 180° rotation about an axis directed along the EFG tensor PAS X-axis (red).

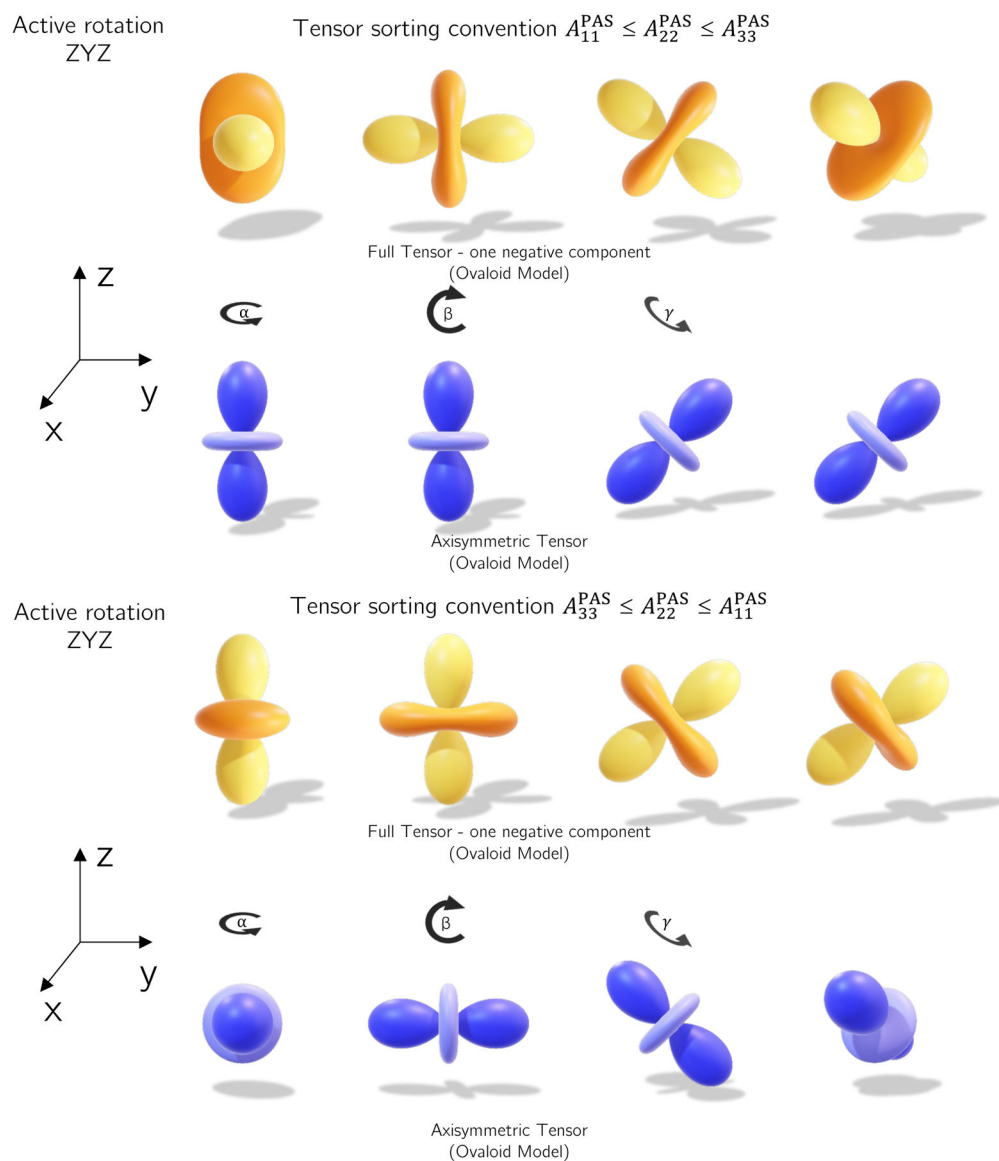


Fig. 6. Sequence of ZYZ active rotations using two different sorting conventions for chemical shielding tensors $(-83, 44, 67)$ ppm $(A_{11}^{\text{PAS}}, A_{22}^{\text{PAS}}, A_{33}^{\text{PAS}})$ ascending sort and an axially symmetric tensor $A_{11}^{\text{PAS}} = A_{22}^{\text{PAS}}$. Only the top “ascending eigen value tensor” obtain rotation on the symmetry axis for the axially symmetrical tensor.

Table 1

ZXZ rotation simplifications for relative orientations of two axi-symmetrical tensors.

ZXZ	α	β	γ
unique B_{33}^{PAS}	90°	$\sin^{-1}\left(\pm\sqrt{\frac{B_{33}^{\text{A}} - B_{33}^{\text{PAS}}}{B_{11}^{\text{PAS}} - B_{33}^{\text{PAS}}}}\right)$	0
unique B_{11}^{PAS}	0	90°	$\sin^{-1}\left(\pm\sqrt{\frac{B_{33}^{\text{A}} - B_{33}^{\text{PAS}}}{B_{11}^{\text{PAS}} - B_{33}^{\text{PAS}}}}\right)$

Author Manuscript

Author Manuscript

Author Manuscript

Author Manuscript